THE JOURNAL OF PHYSICAL CHEMISTRY C

Article

pubs.acs.org/JPCC

Insight into the Adsorption of Water on the Clean CeO_2(111) Surface with van der Waals and Hybrid Density Functionals

Delia Fernández-Torre,[†] Krzysztof Kośmider,[†,‡] Javier Carrasco,[§] M. Verónica Ganduglia-Pirovano,[§] and Rubén Pérez*[,†]

[†]Departamento de Física Teórica de la Materia Condensada, Universidad Autónoma de Madrid, E-28049 Madrid, Spain

[‡]Institute of Experimental Physics, University of Wrocław, plac Maksa Borna 9, PL-50-204 Wrocław, Poland

[§]Instituto de Catálisis y Petroleoquímica, CSIC, C/Marie Curie 2, E-28049 Madrid, Spain

ABSTRACT: Understanding the interaction between water and ceria surfaces is crucial in many catalytic applications. For the clean CeO_2(111) surface, density functional theory (DFT) calculations using different generalized gradient approximations (GGAs) to the exchange-correlation functional and the DFT(GGA)+*U* method have found that the most stable configuration is on top of a surface cerium atom. However, they disagree on the nature of the adsorption state, with water molecularly adsorbed with one or two O_s−H hydrogen bonds (O_s indicates a surface oxygen atom) or as a hydroxyl pair (O_sH_{ads}−OH_{ads}), with only one recent report suggesting that these two structures are very close in energy. In this work, we studied the adsorption of water on CeO_2(111) employing different approximations to exchange and correlation within DFT, namely, the Perdew−Burke−Ernzerhof (PBE) GGA, DFT(PBE)+*U*, the Heyd−Scuseria−Ernzerhof (HSE06) hybrid functional, and van der Waals (vdW) density functionals [DFT(vdW-DF/vdW-DF2)+*U*] with optimized exchange functionals (for vdW-DF, optB86b, revPBE, and optPBE; for vdW-DF2, rPW86). All of these methods predict close energies (10−100 meV range) for the two lowest-energy structures, the molecular structure with one O_s−H bond and the hydroxyl pair. Our calculations show that these two species should be distinguishable by their infrared (IR) spectra. In particular, a rocking libration at 850 cm^{-1} could be used as an IR fingerprint to reveal the presence of the molecular structure. We found that the inclusion of vdW interactions increases binding energies by ∼0.18 eV, bringing them closer to the available experimental values.

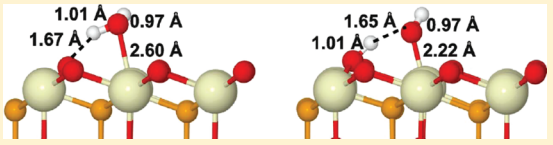

1. INTRODUCTION

Ceria is a key component of many industrial catalysts and a prospective material for fuel cell technology.[1,2] Water is impossible to exclude from realistic environments; thus, knowledge of its behavior on ceria surfaces is important. Moreover, in many catalytic applications, such as the water−gas shift reaction, for which ceria-based systems are promising catalysts,[3−6] the dissociation of water is essential. This has been the motivation for many research works focused on understanding the interaction between water and CeO_2 surfaces at the atomic scale.[7−17] In particular, the thermodynamically most stable CeO_2(111) surface has garnered most of the attention.

The H_2O/CeO_2(111) system has been studied experimentally using X-ray photoelectron spectroscopy (XPS) combined with temperature-programmed desorption (TPD) on a 500-Å epitaxial CeO_2(111) film grown on yttria-stabilized ZrO_2(111)[7] and atomically resolved noncontact atomic force microscopy (nc-AFM) on the (111) surface of ceria single crystals at room temperature.[8,9] Moreover, adsorbed water was identified in a recent low-temperature scanning tunneling microscopy (STM) study of ultrathin ceria films on Pt(111) (see Figure 3 in ref 16). In the room-temperature AFM and low-temperature STM experiments, water was identified as bright triangular protrusions in the images. These triangular features are centered on top of Ce^{4+} ions in the second layer, encompassing the three neighboring O_s sites. Water was not observed in previous STM studies of the CeO_2(111) single-crystal surface, presumably because of the elevated temperatures employed to overcome the insulating nature of ceria. These studies concluded that water does *not* undergo complete dissociation on clean ceria surfaces.

The assignment to hydroxyl groups of some contrast features in nc-AFM[9] and STM[16] images of reduced ceria surfaces suggests that water might dissociate if oxygen vacancies are present. However, TPD and XPS studies have indicated that no dissociation occurs on reduced surfaces. In particular, in ref 7, the TPD spectra for water adsorbed on oxidized and reduced surfaces were compared, and the fact that, in both cases, most of the water (<1 ML) desorbed below room temperature was used as an indication of the desorption of molecularly adsorbed water (see also ref 17). Furthermore, H_2 TPD spectra, which show no evidence for H_2 desorption from water decomposition, and plots of H_2O TPD peak area data as a function of exposure, which show similar near-unity sticking coefficients and no irreversible adsorbed water on either surface (both linear fits pass close to the origin), have been used as indications that both surfaces are unreactive for water decomposition under ultra-high-vacuum conditions. Finally, XPS shows that water

Received: December 30, 2011
Revised: May 12, 2012
Published: May 22, 2012

   dx.doi.org/10.1021/jp212605g | *J. Phys. Chem. C* 2012, 116, 13584−13593

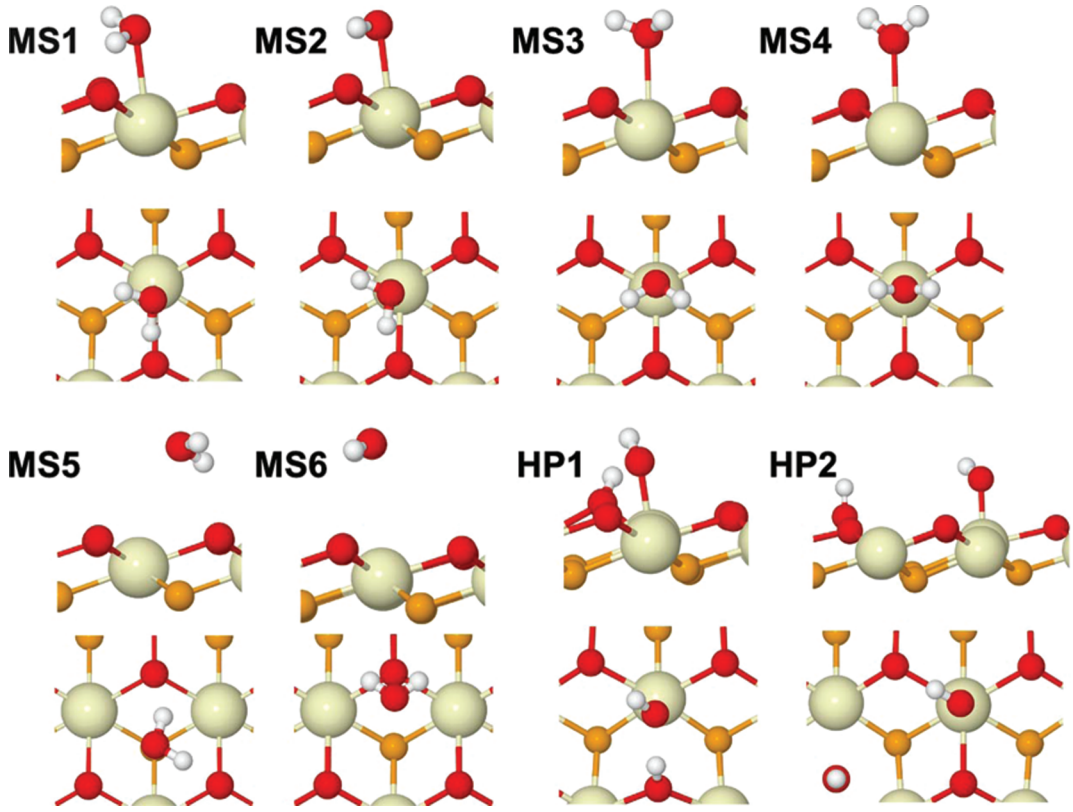

Figure 1. Top and side views of adsorption sites considered for a water molecule (MS1−MS6) and for an O_sH_{ads}−OH_{ads} hydroxyl pair (HP1 and HP2) on $CeO_2(111)$. In structures HP1 and HP2, the O_s atom is nearest and next-nearest neighbors of the surface Ce atom on top of which water adsorbs. Color code: Red, pale yellow, and white balls correspond to O, Ce, and H atoms, respectively. For the sake of clarity, the subsurface O atoms are represented by orange balls.

exposure at 170 K does not result in any noticeable changes in the Ce 3d core-level or Ce 4f valence-band features associated with Ce^{3+}. On the contrary, a similar treatment at 650 K increases the level of surface reduction. In summary, TPD uptake measurements, H_2 TPD data, and XPS spectra support the conclusion that little or no irreversible water dissociation or Ce^{3+} oxidation takes place on the reduced surface.[7]

From the AFM studies, a strong molecule−surface interaction with an estimated barrier of ∼1 eV for diffusion across the Ce sublattice has been concluded. This value can be taken as a lower bound for the binding energy, the energy cost of completely removing the molecule from the substrate. A more rigorous estimate is provided by the desorption energy at low water coverage of ∼0.9 eV obtained from TPD measurements using a Redhead analysis.[18,19]

In the past few years, several theoretical studies of the H_2O/$CeO_2(111)$ system have also been published.[10−12,14,15] The most often considered structures are schematically shown in Figure 1. The conclusions of those works (see Table 1) differ in their predictions of the nature and structure of the thermodynamically most stable configuration of H_2O on $CeO_2(111)$. All of those calculations were based on density functional theory (DFT) and used the generalized-gradient approximation (GGA) for the exchange-correlation functional. In some cases,[12,15] they employed the GGA+*U* method,[20] where a Hubbard-like *U* term describing the on-site Coulomb corrections is added to the GGA functional to enable the description of the case in which the f-orbital overlaps are small, the bands are narrow, and the electrons are nearly localized. Notice that such an approach, mandatory for the description of reduced ceria,[21] might also be relevant for the study of the $H_2O/CeO_2(111)$ system. The result of complete water dissociation is the presence of two hydroxyl groups on the surface: the OH fragment from water adsorbed on the Ce site (OH_{ads}) and the H fragment adsorbed on one of the surface oxygen (O_s) sites forming the O_sH_{ads} group. The H atom in either of those hydroxyl groups could donate its electron to one of the neighboring Ce atoms, creating a surface Ce^{3+} ion.

Kumar and Schelling[10] predicted molecularly adsorbed water with one O_s−H hydrogen bond to be the most stable structure (MS1 in Figure 1), whereas Chen et al.[11] and Fronzi et al.[14] favored the formation of two hydrogen bonds (MS2 in Figure 1). On the contrary, Watkins et al.[12] found a predissociated structure, namely, a spatially confined O_sH_{ads}−OH_{ads} hydroxyl pair (HP1 in Figure 1), energetically favored by 0.3 eV compared to molecular adsorption and by 0.5 eV compared to a (complete) dissociated structure (HP2 in Figure 1). Finally, Yang et al.[15] recently reported the closeness in energy of the MS1 and HP1 structures (20 meV, Table 1), so that both structures should be considered as possible stable configurations for the ground state. The difficulties of finding a DFT answer to the basic question about the adsorption structure might be related to the complexity of the potential energy surface, with many local minima and saddle points, and to the major problem of DFT: the exact functionals for exchange and correlation are not known. A way to overcome these two problems is to perform extensive searches in the configurational space by using the best DFT-based methods available nowadays, and this was our objective in the present work.

DFT+*U* has been applied extensively to study clean and reduced cerium oxide surfaces,[21−24] and its relative merits and

dx.doi.org/10.1021/jp212605g | J. Phys. Chem. C 2012, 116, 13584−13593

Table 1. Adsorption Energies (E_{ads} in eV) for the Stable Configurations of H_2O on $CeO_2(111)$ Obtained with Different Exchange-Correlation Functionals and Unit Cells[a]

ref	method	unit cell	MS1	MS2	MS3	HP1	HP2
Kumar and Schelling[10]	PW91	2×1	−0.58	—	—	—	—
Chen et al.[11 b]	PW91	$\sqrt{3} \times 1$	−0.49	−0.52	—	—	—
Watkins et al.[12]	PW91	$2 \times \sqrt{2}$	—	—	−0.35	−0.65	−0.15
Watkins et al.[12]	PW91+U(5 eV)	$2 \times \sqrt{2}$	—	—	−0.36	−0.66	−0.16
Fronzi et al.[14 c]	PBE	2×2	—	−0.49	−0.33	−0.36	—
Yang et al.[15]	PBE+U(5 eV)	2×2	−0.57	—	—	−0.55	—
this work	PBE	2×2	−0.50	—	—	−0.45	−0.24
this work[d]	PBE+U(4.5 eV)	2×2	−0.54	−0.51[e]	−0.32[f]	−0.52	−0.24
this work	PBE+U(4.5 eV)	3×3	−0.55	—	—	−0.60	−0.17
this work[g]	HSE06	2×2	−0.49	—	−0.30	−0.47	−0.24
this work	revPBE-vdW+U	2×2	−0.54	—	—	−0.45	—
this work	revPBE-vdW+U	3×3	−0.54	—	—	−0.51	−0.17
this work	rPW86-vdW2+U	2×2	−0.60	—	—	−0.49	—
this work	rPW86-vdW2+U	3×3	−0.60	—	—	−0.54	−0.16
this work	optPBE-vdW+U	2×2	−0.67	—	—	−0.61	—
this work	optPBE-vdW+U	3×3	−0.67	—	—	−0.67	−0.23
this work	optB86b-vdW+U	2×2	−0.72	—	—	−0.70	—
this work	optB86b-vdW+U	3×3	−0.73	—	—	−0.76	−0.32

[a]In our calculations, all structures are local minima unless otherwise noted. Other authors are likely not to have investigated the stability of the different structures. [b]For structure MS4 (Figure 1), E_{ads} = −0.19 eV. [c]For structures MS5 and MS6 (Figure 1), E_{ads} = −0.18 and −0.33 eV, respectively. [d]For structure MS5, E_{ads} = −0.12 eV. Structures MS4 and MS6 were unstable and relaxed to MS3 and MS1 respectively. [e]Transition state structure, see Figure 1. [f]Transition state structure. [g]For structure MS5, E_{ads} = −0.15 eV.

shortcomings are well documented. Admittedly, the U term improves the description of Ce atoms in a trivalent configuration, but structural and electronic properties as well as values of reaction energies can depend on the specific method implementation, in particular, the choice of the projector functions used to define the subspaces treated for localized correlation effects, the particular flavor of the underlying GGA functional, and the actual value of the effective Coulomb parameter U.[25−28] Moreover, GGA and GGA+U functionals do not account properly for van der Waals (vdW) dispersion forces, which could play a significant role in stabilizing water−ceria interactions. Finally, differences in the surface unit cell used to model the isolated water molecule can have an effect on the computed adsorption energy values.

In this work, we report a study of the $H_2O/CeO_2(111)$ system using (2×2) and (3×3) surface unit cells, with the hybrid HSE06 functional,[29] in which a fixed amount of nonlocal Fock exchange is added to GGA and different van der Waals-corrected density functionals,[30,31] and the results are compared with those obtained with the GGA and GGA+U. We show that *all* of the methods point to the same answer, already anticipated by Yang et al.[15] with GGA+U: water on clean $CeO_2(111)$ can be found in two states, namely, as a molecule, forming one hydrogen bond with a surface oxygen atom, and as a hydroxyl pair. We discuss the structures, vibrational properties, and adsorption energies and compare our results with previous experimental and theoretical works. To complement this study, we analyzed the activation barrier between the molecular and predissociated states, as well as the rotation of the water molecule.

2. COMPUTATIONAL DETAILS

We have performed spin-polarized calculations using the Vienna ab initio simulation package (VASP, version 5.2.12) with the projector-augmented wave (PAW) method and a cutoff of 500 eV (unless otherwise noted).[32−34] We treated explicitly the Ce (4f, 5s, 5p, 5d, 6s) and O (2s, 2p) electrons as valence states, whereas the remaining electrons were kept frozen as core states in the PAW method. We used different approximations to exchange and correlation within the DFT framework to study the adsorption of water on the clean $CeO_2(111)$ surface. We employed the DFT+U approach of Dudarev et al.,[20] in which a Hubbard U-like term ($U_{eff} = U - J$, i.e., the difference between the Coulomb U and exchange J parameters, hereinafter referred to as U) is added to the Perdew−Burke−Ernzenhof (PBE) gradient-corrected functional.[35] The computational demand of this pragmatic approach compares to that of conventional GGA functionals. Here, we used a value of U = 4.5 eV. Our chosen value of U is equal to the one calculated self-consistently by Fabris et al.[36] using the linear response approach of Cococcioni and de Gironcoli[37] and is within the range of 3.0−5.5 eV reported to provide localization of the electrons left upon oxygen removal from CeO_2.[25]

We also used the Heyd−Scuseria−Ernzerhof (HSE06) hybrid functional with 25% (short-ranged) exact exchange[29] that has been previously applied to fully reduced bulk ceria, Ce_2O_3,[27] and to partially reduced ceria surfaces.[22,38] Hybrid functionals are computationally much more demanding than DFT+U, so we performed non-spin-polarized calculations with a lower cutoff (400 eV). Hybrid-DFT approaches are free from the problems associated with the implementation of the DFT+U method mentioned in section 1; however, results do depend on the admixed amount of exact exchange. In addition, we also considered PBE for the purpose of comparison.

van der Waals (vdW) dispersion forces upon water adsorption on the $CeO_2(111)$ surface might play some role in stabilizing adsorbate−surface interactions. Neither the GGA/GGA+U nor the hybrid functionals account properly for these nonlocal correlations. Different approaches have been developed so far to treat this complex problem.[30,39−51] Although the development of accurate methods to account for vdW forces is still an ongoing quest, one promising and efficient scheme is the nonlocal vdW-DF by Dion et al.[30] and its offspring.[31,48]

dx.doi.org/10.1021/jp212605g | J. Phys. Chem. C 2012, 116, 13584−13593

Table 2. Characteristic Distances for the Two Lowest-Energy Structures of H_2O on $CeO_2(111)$ Obtained Using Different Functionals and Unit Cells (cf. Figure 2)

method		MS1				HP1			
	$a_0(CeO_2)$	OH1	OH2	O_sH2	CeO	OH1	OH2	O_sH2	CeO
PBE, 2 × 2	5.47	0.98	0.99	1.99	2.63	0.97	1.65	1.01	2.22
PBE+*U*, 2 × 2	5.49	0.97	1.01	1.69	2.62	0.97	1.64	1.01	2.23
PBE+*U*, 3 × 3		0.97	1.01	1.67	2.60	0.97	1.65	1.01	2.22
HSE06, 2 × 2	5.39	0.97	0.99	1.78	2.58	0.96	1.67	0.99	2.18
optB86b-vdW+*U*, 2 × 2	5.49	0.98	1.01	1.73	2.59	0.97	1.63	1.01	2.23
optB86b-vdW+*U*, 3 × 3		0.98	1.01	1.71	2.59	0.97	1.66	1.01	2.22
revPBE-vdW+*U*, 2 × 2	5.49	0.97	0.99	1.96	2.70	0.97	1.78	1.00	2.24
revPBE-vdW+*U*, 3 × 3		0.97	0.99	1.91	2.68	0.97	1.75	0.99	2.24
rPW86-vdW+*U*, 2 × 2	5.49	0.98	0.99	2.08	2.68	0.97	1.78	0.99	2.26
rPW86-vdW+*U*, 3 × 3		0.97	0.99	1.94	2.66	0.97	1.76	0.99	2.25
optPBE-vdW+*U*, 2 × 2	5.49	0.98	1.00	1.84	2.64	0.97	1.70	1.00	2.23
optPBE-vdW+*U*, 3 × 3		0.98	0.99	1.80	2.63	0.97	1.70	1.00	2.23

The accuracy of the original vdw-DF[30] can be improved significantly by substituting its underlying exchange functional (revPBE)[52] by other optimized vdW density functionals as reported in ref 48, reaching better-than-chemical accuracy (less than 43 meV) for the S22 data set[42] and now been successfully applied to a variety of systems ranging from solids,[50,53] adsorption of molecules and atoms on surfaces,[54−59] and gas-phase clusters.[48] Specifically, we report herein results of vdW-DF+*U* (a Hubbard-like *U* term added to the vdW-DF) calculations using the original Dion et al. vdW-DF with the revPBE (referred to as revPBE-vdW+*U* herein) and with alternative exchange functionals, namely, optPBE[48] and optB86b.[50] Moreover, we also consider the vdW-DF2 functional[31] with the rPW86[60] exchange, referred by us as rPW86-vdW2+*U*. In VASP, vdW-DF/vdW-DF2 functionals have been implemented by Klimeš et al.[50] using the algorithm of Román-Pérez and Soler.[61]

CeO_2 crystallizes in a cubic fluorite structure (face-centered cubic, $Fm\bar{3}m$). We optimized its lattice constant using PBE, PBE+*U*, and HSE06 (see the resulting values in the first column of Table 2). As previously reported,[27] the lattice constant is slightly underestimated (∼0.4%) with HSE06 and overestimated with PBE (∼1.1%) and PBE+*U* (∼1.5%) compared to the experimental value (5.41 Å).[62−64] These values were used to construct the slabs representing the $CeO_2(111)$ surface. The lattice constant used in the vdW-DF+*U*/vdW-DF2+*U* calculations corresponds to the PBE+*U* value. In all cases, these slabs were nine atomic layers thick with a vacuum space of at least 10 Å. The six top atomic layers of the ceria support were allowed to fully relax, whereas the three bottom layers were kept fixed in their bulk positions. We corrected the leading errors due to dipole−dipole interactions along the direction perpendicular to the slab[65,66] as implemented in the VASP code.

To simulate water adsorption, we first modeled gas-phase water by placing a single molecule in a square box of 10 Å and used the Γ point only to sample the Brillouin zone. Then, we placed an intact H_2O molecule, a hydroxyl pair, and a dissociated molecule close to the outermost layer of one side of the slab in different initial positions and orientations (cf. Figure 1) and relaxed the positions of the molecule and the six top atomic layers using a conjugate-gradient algorithm until the forces were less than 0.01 eV/Å (with DFT, DFT+*U*, and vdW-DF+*U*) or 0.04 eV/Å (with the hybrid functional). Total energies were converged better than 10^{-4} eV per unit cell in the self-consistent-field (SCF) cycle during geometry optimization. The rest of the technical parameters are identical to those used in refs 22 and 27, where they were shown to provide an accurate description of the ceria bulk and surface. We used two different surface periodicities, namely, (2 × 2) and (3 × 3) unit cells with corresponding 3 × 3 × 1 and 2 × 2 × 1 Monkhorst−Pack meshes for the *k*-point sampling (DFT, DFT+*U*, vdW-DF+*U*). The hybrid calculations were done for the (2 × 2) cell with Γ-point sampling for geometry optimization. Single-point calculations with a 2 × 2 × 1 *k* mesh at the geometries of the Γ-point optimizations were performed to obtain total energies.

Vibrational frequencies and the normal modes were obtained by diagonalization of the (full) mass-weighted force-constant matrix in Cartesian coordinates (Hessian). The force constants were obtained from finite differences of the forces with atomic displacements of ±0.01 Å. The bottom O−Ce−O trilayer was kept fixed in the calculation of the vibrational frequencies.

After diagonalization of the Hessian matrix one obtains the corresponding harmonic frequencies, ω^k, and associated normal vibrational modes, Q_k, together with its mass-weighted coordinate matrix, $P_{ki}/(m_i)^{1/2}$. Infrared (IR) intensities for each normal mode, I^k, are directly related to the square of the first derivative of the *z* component of the dynamic dipole moment, $d\mu_z/dQ_k$, which was again evaluated in the Cartesian coordinate system r_i by finite differences $(\partial\mu_z/\partial r_i)$ as

$$I^k \propto \left(\frac{d\mu_z}{dQ_k}\right)^2 = \left(\sum_i^{3N} \frac{P_{ki}}{\sqrt{m_i}} \frac{\partial\mu_z}{\partial r_i}\right)^2 \quad (1)$$

The computed spectra were smoothed by folding with a Gaussian with a half-width of 100 cm^{-1} as follows

$$I(\omega) = \sum_k I^k \exp[-0.01(\omega^k - \omega)^2] \quad (2)$$

The transition-state (TS) structures for relevant processes were located by employing the climbing image nudged elastic band (CI-NEB) method[67] using five images along each pathway. All TS structures were characterized by vibrational analysis. Both the vibrational frequencies and energy barrier calculations were performed with the PBE+*U* approximation on a (2 × 2) unit cell.

3. STRUCTURES AND ADSORPTION ENERGIES

Using a (2 × 2) unit cell with one water molecule, we considered various adsorption configurations, namely, molecular (MS1−MS6), hydroxyl pair (HP1), and dissociative (HP2) with PBE+*U* (cf. Figure 1). Table 1 gives the values of the

dx.doi.org/10.1021/jp212605g | J. Phys. Chem. C 2012, 116, 13584−13593

adsorption energies for the three molecular configurations with higher binding (MS1−MS3), as well as HP1 and HP2. Structures MS4 and MS6 did not correspond to real energy minima in our calculations and, upon relaxation, converted into MS3 and MS1, respectively. Structure MS5 is approximately 0.4 eV less stable than MS1. The MS2 and MS3 configurations correspond to transition structures because one of the vibrational eigenvalues is negative in each case (see section 5). It can be seen that the two most favorable structures are MS1 and HP1, with an energy difference of ∼20 meV [∼10 meV with zero-point-corrected energies: −0.46 (MS1) and −0.47 (HP1)], and the dissociated HP2 structure is by about 0.3 eV less stable. Also, in previous PBE+*U* calculations with the same unit cell,[15] the closeness in energy between the MS1 and HP1 structures was reported. We found that using a (3 × 3) unit cell with one water molecule did not qualitatively change this finding (∼50 meV difference). Thus, the different choice of unit cell does not play a significant role in the relative stabilization of these structures.

Figure 2 shows water in the MS1 and the HP1 structures as obtained with the (3 × 3) cell. In the MS1 configuration, water

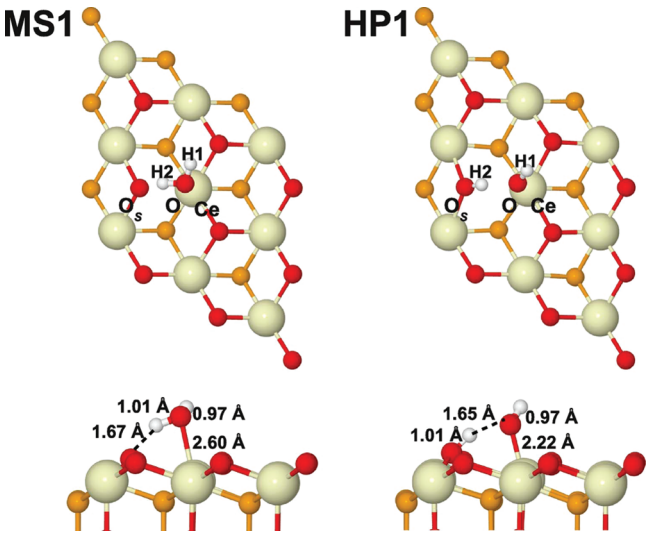

Figure 2. Top and side views of the most stable structures [PBE+*U*, (3 × 3) surface unit cell] for molecular adsorption (MS1) and hydroxyl-pair formation (HP1). Selected interatomic distances are indicated. The dashed black lines denote hydrogen bonds. Color code as in Figure 1.

adsorbs molecularly on top of a Ce^{4+} ion with a slight asymmetry in the O−H distances [0.97 Å (OH1) and 1.01 Å (OH2); cf. Figure 2 and Table 2]. The molecular plane is nearly parallel to the surface, and one of the O−H bonds (OH2) is tilted downward, pointing toward a neighboring surface oxygen (O_s), forming a hydrogen bond [∼1.67 Å (O_sH2), (3 × 3) unit cell]. The distance between the O atom in H_2O and the closest Ce atom is 2.60 Å, which is about 9% greater than the Ce−O distance in bulk CeO_2 (2.38 Å, PBE+*U*). In the HP1 configuration, water is predissociated, forming a hydroxyl pair confined in the neighborhood of a Ce^{4+} ion (Figure 2). The O_s−H2 and O−H1 distances are 0.97 and 1.01 Å, respectively, and the Ce−O distance is 2.22 Å. We note the strong relaxation of O_s in both structures. For molecularly adsorbed water, O_s has moved upward by ∼0.12 Å and in the surface plane, away from the Ce ion, by ∼0.24 Å, whereas for the hydroxyl pair, the corresponding O_s displacements are about 3 times larger.

Inspection of the density of states (not shown) does not suggest a net charge transfer between molecule and surface; that is, no $Ce^{4+} \rightarrow Ce^{3+}$ reduction occurs upon water adsorption on clean CeO_2(111). Thus, it is not two surprising that PBE (without *U* corrections) and PBE+*U* perform similarly (cf. Tables 1 and 2).

The HSE06 hybrid DFT calculations with a (2 × 2) suface unit cell provide the same results as PBE+*U* for relative energies between the MS1, HP1, and HP2 configurations (cf. Table 1): MS1 and HP1 are separated by a relatively small energy difference (∼20 meV), and HP2 is significantly less stable (∼0.3 eV). The adsorption geometries present some differences compared to those obtained with PBE+*U*, particularly for the MS1 configuration (Table 2). The asymmetry in the O−H bonds (OH1, OH2) is less pronounced, and the hydrogen bond (O_sH2) is somewhat weaker.

We further considered the van der Waals density functionals, namely, vdW-DF with the optB86b, revPBE, and optPBE exchange functionals and vdW-DF2 with the rPW86 functional, in combination with a Hubbard-like *U* term. As predicted by the PBE+*U* and HSE06 functionals, the energy difference between the MS1 and HP1 configurations lies within approximately a 10−100 meV range. The different choice of unit cell with the vdW+*U* functionals does not play a significant role in the relative stabilities of the two relevant structures. We note that, consistently with PBE+*U* and HSE06, the dissociated HP2 structure is also significantly less stable than both the molecular MS1 and hydroxyl-pair structures [0.2−0.4 eV, (3 × 3) unit cell]. Hence, if the energy barrier between the MS1 and HP1 structures is not too large, one can expect both states to be similarly populated, even at low temperature. We will discuss this point in more detail in section 5. Here, we considered the vdW-DF/vdw-DF2 adsorption geometries of the MS1 and HP1 structures. In Table 2, selected interatomic distances for the optB86b-vdW+*U*, revPBE-vdW+U, optPBE-vdW+U, and rPW86-vdW2+U functionals are listed. The largest variations with the choice of functional are observed for the O_s−H2 and Ce−O bonds of the MS1 structure, which lie at about 0.35 and 0.11 Å, respectively, in a (2 × 2) unit cell. Considering a (3 × 3) cell, the variations are somewhat smaller [0.23 Å (O_sH2) and 0.09 Å (CeO), Table 2].

From the results presented so far, we conclude that all methods consistently predict that complete water dissociation (HP2) is not favorable and that the molecular (MS1) and hydroxyl-pair (HP1) structures are very close in energy. The stability of the MS1 and HP1 structures was recently reported for a number of (001) surfaces of metal oxides such as CaO, SrO, BaO, and SrO-terminated $SrTiO_3$.[54,68−70] However, in all of these cases, one of the two states is clearly more stable than the other. For example, the HP1 state is preferred on CaO, SrO, BaO, and SrO-terminated $SrTiO_3$, whereas the MS1 state dominates on MgO. Interestingly, we show that, on CeO_2(111), the two states compete in energy and, therefore, the two configurations are expected to coexist.

We believe that this particular behavior can be understood in terms of some of the trends that were identified in previous studies of the adsorption and dissociation of water on oxides.[54,68] The interaction strength and the preferred adsorption geometry result from a competition between (i) the electrostatic interaction of the oxygen atom in water with the surface cation and (ii) the hydrogen bonding of H atoms with the neighboring oxygen sites.[54] There are no significant differences in the charge state of the adsorbed molecule or in the hydroxyl groups created upon dissociation among the different oxides, so we focused on the

dx.doi.org/10.1021/jp212605g | J. Phys. Chem. C 2012, 116, 13584−13593

contribution of the H-bonding. In this interaction, bond distance correlates with bond strength: shorter hydrogen bonds are stronger.[54] From this perspective, the key for the coexistence of the two adsorption states in ceria is that the corresponding H-bond distances in these structures, O_sH2 for the molecular (MS1) state and OH2 (i.e., the distance between the H transferred to the O_s site and the oxygen atom in the hydroxyl group that is bonded to the Ce ion) for the dissociated (HP1) state, are very close: 1.67 versus 1.65 Å for PBE+*U* and 1.71 versus 1.66 Å for optB86b-vdW+U. Thus, there is no significant difference in the strength of the H-bond if the H atom is attached to the O in the water molecule or the O_s atom in the surface. The similarity between the H-bond distances is probably related to the lattice parameter and crystal structure of ceria, which enable the adsorbed species to be at the right distances from the surface cation and the surrounding O atoms, but also to the "geometric flexibility" of the (111) surface. This factor has been identified as one of the key parameters controlling water dissociation.[54] The $CeO_2(111)$ surface seems indeed to be flexible enough (the relaxation of O_s is quite large) to allow dissociation and, at the same time, sustain the formation of an optimal H-bond with the surface O_s atom that stabilizes the molecular MS1 state. The OH2 distance in our HP1 state (1.65 Å, PBE+*U*) lies between the values found in PW91 calculations for other oxide surfaces such as CaO(001) (1.55 Å) and BaO(001) (1.74 Å), where water clearly dissociates into a hydroxyl pair.[68] On the other hand, the O_sH2 distance for our MS1 configuration (1.67 Å, PBE+*U*) is 0.22 Å shorter than in the MgO(001) case (1.88 Å), where only the molecular adsorption state is stable.

Having identified the relevant structures for the ceria−water system, we discuss the effect of vdW interactions on the adsorption energy value. According to PBE+*U* and HSE06, the adsorption energies for both the MS1 and HP1 structures are approximately 0.45−0.55 eV in a (2 × 2) cell. Inclusion of vdW interactions using the most accurate vdW-DF considered (optB86b-vdW+*U*) yields adsorption energies that are in the 0.70−0.76 eV range for both (2 × 2) and (3 × 3) cells. As PBE+*U* and HSE06 do not account for vdW interactions, we found the results obtained with the vdW+*U* approaches to be most reliable. Comparing, in particular, the PBE+*U* and the optB86b-vdW+*U* results, an additional contribution of ∼180 meV to the binding energy is found. This value is consistent with the vdW contribution per water molecule calculated recently for a one-dimensional water chain adsorbed on Cu(110) (∼150 meV) and a two-dimensional water overlayer on Ru(0001) (180 meV).[56] An adsorption energy of ∼0.7 eV is in fair agreement with the most accurate experimental result available, namely, the estimated[18,19] desorption energy at low water coverage of ∼0.9 eV from TPD measurements.[7]

We note that, among the different vdW functionals with exchange functionals optimized for the correlation part considered in this work, optB86b-vdW is probably the best balanced and, therefore, most accurate. The overestimation of the revPBE-vdW (and to a less extent rPW86-vdW2) binding distances, observed systematically for many systems,[30,31,48,50,71−75] is reduced in the case of the optB86b-vdW functional, because the latter is designed to be less repulsive for distances larger than equilibrium.[50] Moreover, compared with other optimized functionals such as optPBE-vdW, the optB86b-vdW functional presents a smaller error cancellation between exchange and correlation.[50]

Having established that all of the tested methods (GGA, GGA+*U*, HSE06, and vdW-DF+*U*) predict the closeness in energy (10−100 meV range) of the molecular structure with one O_s−H bond (MS1) and the hydroxyl pair (HP1) and that the result is robust with respect of the choice of the surface unit cell, (2 × 2) and (3 × 3), we turn back to the results of previous works[10−12,14,15] and the reasons that finding a DFT answer to the basic question about the adsorption structure has been challenging (see section 1). According to our results, the difficulties are related not to the choices for the exchange-correlation functional and surface unit cell but rather to the complexity of the potential energy surface with many local minima and saddle points. It is likely that Kumar and Schelling[10] and Chen et al.[11] considered neither a hydroxyl pair nor dissociation, as they were strongly motivated by TPD studies that discarded water dissociation and pointed to three different configurations of the water molecule adsorbed on top of a surface cerium atom.[7] Fronzi et al.[14] favored the formation of the molecular structure with two hydrogen bonds (MS2 in Figure 1), with the HP1 structure separated by 0.13 eV (cf. Table 1). However, using the same exchange-correlation functional and surface unit cell [PBE, (2 × 2) cell], we found that MS2 quickly relaxes into MS1. Furthermore, we obtained a difference of only 0.05 eV between MS1 and HP1. Given that we used a very similar lattice parameter and that the resulting adsorption structures are also very similar (as shown by comparing the relevant O−H and Ce−O distances), we believe that the disagreement in the energetics can be attributed to limitations of the basis set of atomic-like orbitals used in ref 14. Watkins et al.[12] found the hydroxyl pair energetically favored by 0.3 eV compared to the MS3 molecular adsorption (cf. Table 1). We obtained a very similar adsorption energy for the MS3 structure by employing the same methodology; however, we found that it corresponds to a transition structure. Thus, Watkins et al. missed the lowest-energy structure for molecular adsorption. The latest results of Yang et al.[15] based on PBE+*U* and using a (2 × 2) unit cell showed the adsorption energy difference between the MS1 and HP1 structures to be 20 meV, close to our own values.

4. VIBRATIONAL FREQUENCIES

The vibrational frequency spectra of MS1 and HP1 structures are expected to differ in terms of peak positions and IR intensities, offering the possibility of experimentally characterizing these two structures on the $CeO_2(111)$ surface. Although, to the best of our knowledge, no experimental IR spectra have been reported for isolated water molecules on $CeO_2(111)$, we considered the calculation of the vibrational frequencies of MS1 and HP1 species relevant for comparison with eventual new experimental data. Fronzi et al.[14] computed such frequencies for the MS2 structure, but as discussed previously, this is not an equilibrium geometry but rather a TS according to our calculations (section 5).

In Table 3, we compare the vibrational frequencies of gas-phase water with those of the MS1 and HP1 configurations on $CeO_2(111)$. We also provide a brief description of the vibrational mode associated with each frequency. Both the MS1 and HP1 structures present decoupled O−H stretches, in contrast to the O−H symmetric and asymmetric stretching modes of gas-phase water. The free O−H1 stretch appears at higher wave numbers, whereas the O−H2 (MS1) and O_s−H2 (HP1) stretches are at lower values. In particular, the OH2 (O_sH2) stretch of the MS1 (HP1) configuration shifts substantially—by 690 (730) cm^{-1}—with respect to the O−H symmetric stretch of gas-phase water.

Both the MS1 and HP1 structures show two low frequencies. These features are associated with rather complex multiatom modes involving mainly O, O_s, H1, and H2 atoms (see the insets in Figure 3, in which we use arrows to mark the

dx.doi.org/10.1021/jp212605g | J. Phys. Chem. C 2012, 116, 13584−13593

Table 3. Harmonic Frequencies (in cm^{-1}) for Gas-Phase Water and Molecular (MS1) and Hydroxyl-Pair (HP1) Water on CeO_2(111), along with a Brief Description of Each Vibrational Mode[a]

	H_2O(g)		
	1585	3712	3827
	H−O−H bending vibration	O−H symmetric stretch	O−H asymmetric stretch
	MS1		
851	1552	3025	3762
O_s−O−H2 rocking libration	H1−O−H2 waving libration	O−H2 stretch	O−H1 stretch
	HP1		
897	1008	2986	3794
O_s−H2 twisting libration	O−H1 and O_s−H2 twisting librations	O_s−H2 stretch	O−H1 stretch

[a]Results obtained with PBE+U and a (2 × 2) unit cell.

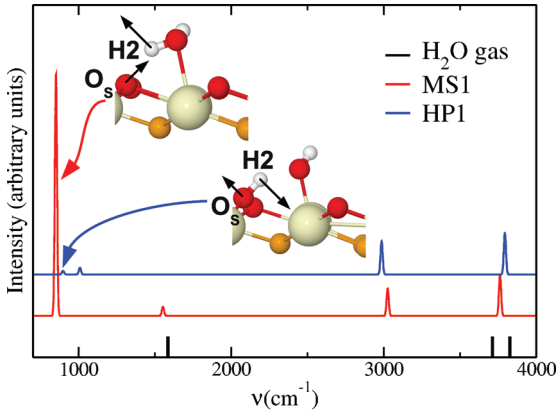

Figure 3. Calculated infrared absorption spectra for gas-phase water and molecular and predissociated water on CeO_2(111). These data correspond to the PBE+U functional and a (2 × 2) unit cell. Intensities are normalized to the peak corresponding to the OH1 stretch.

directions of the largest atomic displacements for some of these modes). We assigned them as rocking-, waving-, and twisting-like librations (see Table 3). When water is molecularly adsorbed (MS1), the waving mode is at 1552 cm^{-1} (similar to the bending mode of gas-phase water), whereas the rocking libration (see the the upper inset in Figure 3) is at a much lower frequency (850 cm^{-1}) and is much more intense (Figure 3). In the case of the hydroxyl pair (HP1), both modes are twisting-like librations of low intensity that are at 1000−900 cm^{-1}.

Interestingly, only the MS1 structure shows a relatively intense IR peak (the rocking libration at 850 cm^{-1}), whereas all of the other modes associated with the MS1 and HP1 configurations are not very intense. Therefore, this peak could be use as an IR fingerprint to reveal the presence of MS1 species on the CeO_2(111) surface. Moreover, an IR probe sensitive enough to record all of these low- and high-frequency vibration modes at the same time could, in principle, be used to confirm the presence (and estimate the proportion) of both MS1 and HP1 species.

5. ENERGY BARRIERS

As a consequence of the symmetry of the CeO_2 (111) surface and the adsorbed species, there are three equivalent configurations for the O_sH_{ads}−OH_{ads} hydroxyl pair (see Figure 1a), which can be obtained by a 3-fold rotation around an axis perpendicular to the surface and passing through the central Ce atom. Note that three additional equivalent configurations can be generated from those structures by reflection on a mirror plane perpendicular to the surface and passing through Ce and O_s (M1, M2 and M3 in Figure 4). Using molecular dynamics simulations, Watkins et al.[12] showed that these three equivalent configurations can be "occupied" at room temperature. They proposed that the triangular protrusions associated with water in the STM and AFM images can be explained in terms of hopping between these three equivalent hydroxyl-pair structures. The mechanism by which the 3-fold rotation occurs involves a transition between the hydroxyl pair and the molecular state with a facile reorientation of the latter. The process is depicted in Figure 4b.

To accurately evaluate the energy barrier between the molecular and hydroxyl-pair states, we performed CI-NEB calculations. Different conceivable transitions were investigated with initial- and final-state atom mappings based on topological similarities, and only the less energetically demanding paths are shown in Figure 4b. A hydroxyl pair can recombine (process labeled RD in the figure) through a small barrier (0.08 eV) to

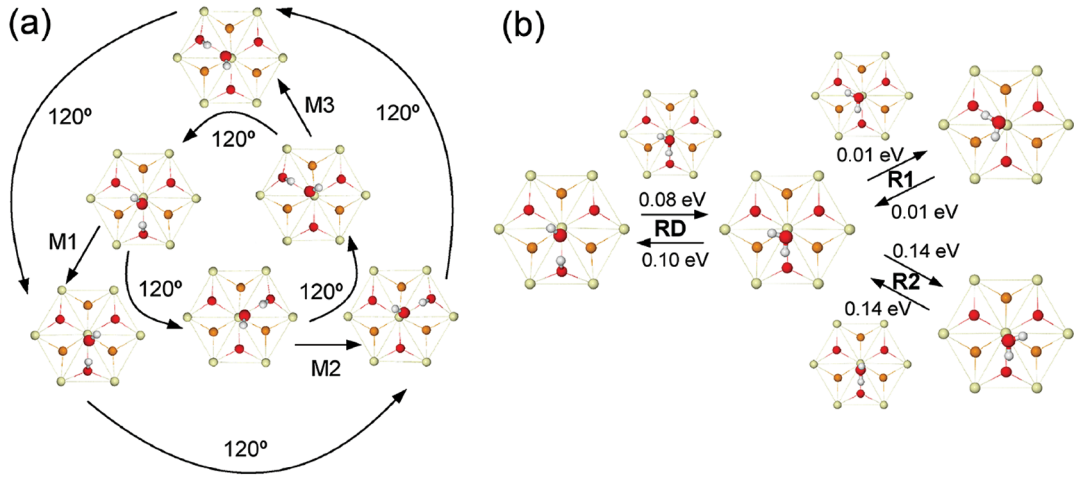

Figure 4. (a) Equivalent structures for the HP1 structure, (b) mechanisms involved in the rotation of the hydroxyl pair. RD: recombination/(partial) dissociation of water. R1, R2: rotation of molecularly adsorbed water. Color code as in Figures 1 and 2.

dx.doi.org/10.1021/jp212605g | J. Phys. Chem. C 2012, 116, 13584−13593

form the MS1 molecular structure; the reverse process is hindered by only a marginally higher barrier (0.10 eV), and therefore, one should expect these two states to coexist even at low temperatures. The water molecule can reorient itself on the surface through two distinct processes, R1 and R2, as shown in Figure 4b. In R1, the hydrogen bond between the tilted water molecule with an O_s atom of the initial structure is broken in the transition structure, but another one forms in the final structure involving the other hydrogen atom and another O_s atom. This process has essentially no barrier (0.01 eV), and the TS corresponds to a completely flat H_2O molecule on the surface (our MS2 structure, see Figure 1). This TS structure has been discussed in previous works, where it was found to be either a stable[11,14] or an unstable[10] structure. In process R2, which has a higher barrier (0.14 eV), the hydrogen bond between water and O_s of the initial structure is preserved in the final structure, with the O−H molecular bond changing its orientation, passing through an upright position in the TS structure.

Overall, we conclude that the three equivalent configurations of the hydroxyl pair are easily accessible through a series of steps: (i) recombination into the molecular state, (ii) processes R1 and R2 involving the reorientation of the molecular water, and (iii) splitting of the molecular water to form an equivalent pair. These reactions are expected to occur even at low temperatures, as the highest energy barrier required is only 0.14 eV (process R2). From this perspective, both the hydroxyl pair (HP1) and the molecular state (MS1) are consistent with the triangular protrusions associated with water in STM and AFM images.

6. CONCLUSIONS

We have performed a comprehensive study of the adsorption of water on clean $CeO_2(111)$ with the hybrid HSE06 functional and different van der Waals-corrected density functionals and compared the results with those obtained with the GGA and GGA+*U* approximations. All of the methods rule out complete water dissociation as the thermodynamically stable phase and show that water adsorbs on top of a Ce^{4+} atom and can be found either in a molecular state (MS1, forming one hydrogen bond with a surface oxygen atom) or as a hydroxyl pair (HP1). These states are very close in energy, with differences in the range of ∼10−30 meV depending on the exchange-correlation functional and unit cell considered, and are separated by an energy barrier of ∼100 meV. We note that a very recent calculation using the DFT+*U* approach with the PW91 exchange-correlation functional obtained very similar results.[76]

In this respect, ceria seems to be different from other oxides, on which one of these two water states is clearly favored. We believe that the key for the coexistence of the molecular and dissociated states on ceria is that the H-bond distances, and thus the bond strengths, are very similar for the two structures. This fact is related to the suitable lattice parameter and crystal structure of ceria, but also to the flexibility of the (111) surface, as surface ions can relax to allow a hydroxyl-pair HP1 configuration and, at the same time, sustain the formation of an optimal H-bond that stabilizes the molecular MS1 state.

The appearance of water in the STM and AFM images as triangular protrusions spanning three O_s sites is consistent with the low barriers found for the interchange of water among the three equivalent configurations that are possible for both the molecular and hydroxyl-pair configurations. This interchange takes place through a combination of different steps involving recombination of the hydroxyl pair, reorientation of the molecular water, and dissociation. These processes are active even at low temperatures, as our CI-NEB calculations show that the highest activation barrier is only 140 meV.

Our results show that the discrepancies among previous theoretical calculations for water on ceria, using different exchange-correlation functionals and unit cells, are essentially related to an incomplete exploration of the phase space. Vibrational analysis confirms that some of the previously proposed structures are not true energy minima. On the other hand, our study shows that a relatively intense IR peak (a rocking libration at 850 cm^{-1}) could be used as an IR fingerprint to reveal the presence of MS1 species on the $CeO_2(111)$ surface. This is particularly important, as the triangular protrusions associated with water in STM and AFM images are consistent with both the hydroxyl-pair and molecular-state structures.

Finally, we have shown that the vdW interactions do not substantially modify the water binding structure but contribute an additional ∼180 meV to the adsorption energy per water molecule, in line with recent calculations for water adsorbed on metal surfaces.[56] This contribution brings the adsorption energy to a final value of ∼0.7 eV, which is in fair agreement with the estimated desorption energy at low water coverage of ∼0.9 eV from TPD measurements[7,18,19] and consistent with the large diffusion barriers (∼0.9 eV) found in AFM studies.[9]

AUTHOR INFORMATION

Corresponding Author

*E-mail: ruben.perez@uam.es.

Notes

The authors declare no competing financial interest.

ACKNOWLEDGMENTS

We thank the Spanish MINECO (Projects MAT2011-23627, MAT2008-02929-NAN, MAT2008-02939-E, PLE2009-0061, and CSD2010-00024), the Comunidad de Madrid (Project S2009/MAT-146), the ESF (AFRI project within the FANAS Eurocores Programme), and the EULANEST Project 042-CERENH2 (MINECO: PIM2010EEUU-00138) for financial support. J.C. was supported by the MINECO through a Ramon y Cajal Fellowship. Computer time provided by the Spanish Supercomputing Network (RES) at the CeSViMa (Madrid), CESGA (Santiago de Compostela), and BSC (Barcelona) is gratefully acknowledged. This work was granted access to the HPC resources of the Rechenzentrum Garching (RZG) made available within the Distributed European Computing Initiative by the PRACE-2IP, receiving funding from the European Union Seventh Framework Programme (FP7/2007-2013) under Grant Agreement RI-283493. We also thank the SGAI-CSIC (Secretaria General Adjunta de Informática−Consejo Superior de Investigaciones Científicas) for computational resources. The authors are grateful to Oscar Custance and Michael Reichling for valuable discussions on the nc-AFM experimental results.

REFERENCES

(1) Trovarelli, A.; de Leitenburg, C.; Boaro, M.; Dolcetti, G. *Catal. Today* **1999**, *50*, 353−367.

(2) Atkinson, A.; Barnett, S.; Gorte, R.; Irvine, J.; Mcevoy, A.; Mogensen, M.; Singhal, S.; Vohs, J. *Nat. Mater.* **2004**, *3*, 17−27.

(3) Fi, Q.; Saltsburg, H.; Flytzani-Stephanopoulos, M. *Science* **2003**, *301*, 2033.
(4) Si, R.; Flytzani-Stephanopoulos, M. *Angew. Chem., Int. Ed.* **2008**, *47*, 2884.
(5) Park, J. B.; Graciani, J.; Evans, J.; Stacchiola, D.; Ma, S.; Liu, P.; Nambu, A.; FernándezSanz, J.; Hrbek, J.; Rodriguez, J. A. *Proc. Natl. Acad. Sci. U.S.A.* **2009**, *106*, 4975.
(6) Rodriguez, J. A.; Ma, S.; Liu, P.; Hrbek, J.; Evans, J.; Pérez, M. *Science* **2007**, *318*, 1757.
(7) Henderson, M.; Perkins, C.; Engelhard, M.; Thevuthasan, S.; Peden, C. *Surf. Sci.* **2003**, *526*, 1−18.
(8) Gritschneder, S.; Iwasawa, Y.; Reichling, M. *Nanotechnology* **2007**, *18*, 044025.
(9) Gritschneder, S.; Reichling, M. *Nanotechnology* **2007**, *18*, 044024.
(10) Kumar, S.; Schelling, P. K. *J. Chem. Phys.* **2006**, *125*, 204704.
(11) Chen, H.-T.; Choi, Y. M.; Liu, M.; Lin, M. C. *ChemPhysChem* **2007**, *8*, 849−855.
(12) Watkins, M. B.; Foster, A. S.; Shluger, A. L. *J. Phys. Chem. C* **2007**, *111*, 15337−15341.
(13) Watkins, M.; Trevethan, T.; Shluger, A. L.; Kantorovich, L. N. *Phys. Rev. B* **2007**, *76*, 245421.
(14) Fronzi, M.; Piccinin, S.; Delley, B.; Traversa, E.; Stampfl, C. *Phys. Chem. Chem. Phys.* **2009**, *11*, 9188−9199.
(15) Yang, Z.; Wang, Q.; Wei, S.; Ma, D.; Sun, Q. *J. Phys. Chem. C* **2010**, *114*, 14891−14899.
(16) Grinter, D. C.; Ithnin, R.; Pang, C. L.; Thorton, G. *J. Phys. Chem. C* **2010**, *114*, 17036.
(17) Henderson, M. *Surf. Sci. Rep.* **2002**, *46*, 1−308.
(18) Redhead, P. A. *Vacuum* **1962**, *12*, 203.
(19) The desorption energy of 0.88 eV at low coverage (0.04−0.07 ML) was estimated using T = 320 K and assuming a preexponential of 10^{13} s^{-1} and a heating rate of 1 K/s.
(20) Dudarev, S.; Botton, G.; Savrasov, S.; Humphreys, C.; Sutton, A. *Phys. Rev. B* **1998**, *57*, 1505−1509.
(21) Ganduglia-Pirovano, M. V.; Hofmann, A.; Sauer, J. *Surf. Sci. Rep.* **2007**, *62*, 219−270.
(22) Ganduglia-Pirovano, M. V.; Da Silva, J. L. F.; Sauer, J. *Phys. Rev. Lett.* **2009**, *102*, 026101.
(23) Li, H.; Wang, H. F.; Gong, X.; Guo, Y.; Guo, Y.; Lu, G.; Hu, P. *Phys. Rev. B* **2009**, *79*, 193401.
(24) Zhang, C.; Michaelides, A.; King, D. A.; Jenkins, S. J. *Phys. Rev. B* **2009**, *79*, 075433.
(25) Castleton, C. W. M.; Kullgren, J.; Hermansson, K. *J. Chem. Phys.* **2007**, *127*, 244704−1−244704−11.
(26) Loschen, C.; Konstantin, J. C.; Neyman, M.; Illas, F. *Phys. Rev. B* **2007**, *75*, 035115−1−035115−8.
(27) Da Silva, J. L. F.; Ganduglia-Pirovano, M. V.; Sauer, J.; Bayer, V.; Kresse, G. *Phys. Rev. B* **2007**, *75*, 045121−1−045121−10.
(28) Fabris, S.; Vicario, G.; Balducci, G.; de Gironcoli, S.; Baroni, S. *J. Phys. Chem. B* **2005**, *109*, 22860−22867.
(29) Krukau, A. V.; Vydrov, O. A.; Izmaylov, A. F.; Scuseria, G. E. *J. Chem. Phys.* **2006**, *125*, 224106−1−224106−5.
(30) Dion, M.; Rydberg, H.; Schröder, E.; Langreth, D.; Lundqvist, B. *Phys. Rev. Lett.* **2004**, *92*, 246401.
(31) Lee, K.; Murray, E. D.; Kong, L.; Lundqvist, B. I.; Langreth, D. C. *Phys. Rev. B* **2010**, *82*, 081101.
(32) Kresse, G.; Furthmüller, J. *Comput. Mater. Sci.* **1996**, *6*, 15.
(33) Kresse, G.; Furthmüller, J. *Phys. Rev. B* **1996**, *54*, 11169−11186.
(34) The VASP site, http://www.vasp.at (accessed June 6, 2012).
(35) Perdew, J.; Burke, K.; Ernzerhof, M. *Phys. Rev. Lett.* **1996**, *77*, 3865−3868.
(36) Fabris, S.; de Gironcoli, S.; Baroni, S.; Vicario, G.; Balducci, G. *Phys. Rev. B* **2005**, *72*, 237102−1−237102−2.
(37) Cococcioni, M.; de Gironcoli, S. *Phys. Rev. B* **2005**, *71*, 035105−1−035105−16.
(38) Nolan, M. *Chem. Phys. Lett.* **2010**, *499*, 126−130.
(39) Wu, Q.; Yang, W. *J. Chem. Phys.* **2002**, *116*, 515−524.
(40) Grimme, S. *J. Comput. Chem.* **2004**, *25*, 1463−1473.
(41) Grimme, S.; Antony, J.; Ehrlich, S.; Krieg, H. *J. Chem. Phys.* **2010**, *132*, 154104.
(42) Jurečka, P.; Černý, J.; Hobza, P.; Salahub, D. R. *J. Comput. Chem.* **2007**, *28*, 555−569.
(43) Becke, A.; Johnson, E. *J. Chem. Phys.* **2005**, *122*, 154104.
(44) Silvestrelli, P. L. *Phys. Rev. Lett.* **2008**, *100*, 053002.
(45) von Lilienfeld, O.; Tavernelli, I.; Rothlisberger, U.; Sebastiani, D. *Phys. Rev. Lett.* **2004**, *93*, 153004.
(46) Tkatchenko, A.; Scheffler, M. *Phys. Rev. Lett.* **2009**, *102*, 073005.
(47) Schimka, L.; Harl, J.; Stroppa, A.; Grueneis, A.; Marsman, M.; Mittendorfer, F.; Kresse, G. *Nat. Mater.* **2010**, *9*, 741−744.
(48) Klimeš, J.; Bowler, D. R.; Michaelides, A. *J. Phys.: Condens. Matter* **2010**, *22*, 022201.
(49) Langreth, D. C.; Lundqvist, B. I.; Chakarova-Käck, S. D.; Cooper, V. R.; Dion, M.; Hyldgaard, P.; Kelkkanen, A.; Kleis, J.; Kong, L.; Li, S.; Moses, P. G.; Murray, E.; Puzder, A.; Rydberg, H.; Schröder, E.; Thonhauser, T. *J. Phys.: Condens. Matter* **2009**, *21*, 084203.
(50) Klimeš, J.; Bowler, D. R.; Michaelides, A. *Phys. Rev. B* **2011**, *83*, 195131.
(51) Kelkkanen, A. K.; Lundqvist, B. I.; Norskov, J. K. *Phys. Rev. B* **2011**, *83*, 113401.
(52) Zhang, Y. K.; Yang, W. T. *Phys. Rev. Lett.* **1998**, *80*, 890.
(53) Santra, B.; Klimeš, J.; Alfè, D.; Tkatchenko, A.; Slater, B.; Michaelides, A.; Car, R.; Scheffler, M. *Phys. Rev. Lett.* **2011**, *107*, 185701.
(54) Hu, X. L.; Carrasco, J.; Klimes, J.; Michaelides, A. *Phys. Chem. Chem. Phys.* **2011**, *13*, 12447−12453.
(55) Floridia Addato, M. A.; Rubert, A. A.; Benitez, G. A.; Fonticelli, M. H.; Carrasco, J.; Carro, P.; Salvarezza, R. C. *J. Phys. Chem. C* **2011**, *115*, 17788−17798.
(56) Carrasco, J.; Santra, B.; Klimes, J.; Michaelides, A. *Phys. Rev. Lett.* **2011**, *106*, 026101.
(57) Zhang, Y. N.; Hanke, F.; Bortolani, V.; Persson, M.; Wu, R. Q. *Phys. Rev. Lett.* **2011**, *106*, 236103.
(58) Lew, W.; Crowe, M. C.; Campbell, C. T.; Carrasco, J.; Michaelides, A. *J. Phys. Chem. C* **2011**, *115*, 23008.
(59) Lawton, T. J.; Carrasco, J.; Baber, A. E.; Michaelides, A.; Sykes, E. C. H. *Phys. Rev. Lett.* **2011**, *107*, 256101.
(60) Murray, E. D.; Lee, K.; Langreth, D. C. *J. Chem. Theory Comput.* **2009**, *5*, 2754.
(61) Román-Pérez, G.; Soler, J. M. *Phys. Rev. Lett.* **2009**, *103*, 096102.
(62) Duclos, S. J.; Vohra, Y. K.; Ruoff, A. L.; Jayaraman, A.; Espinosa, G. P. *Phys. Rev. B* **1988**, *38*, 7755.
(63) Gerward, L.; Olsen, J. S. *Powder Diffr.* **1993**, *8*, 127.
(64) Gerward, L.; Olsen, J. S.; Petit, L.; Vaitheeswaran, G.; Kanchana, V.; Svane, A. *J. Alloys Compd.* **2005**, *400*, 56.
(65) Makov, G.; Payne, M. C. *Phys. Rev. B* **1995**, *51*, 4014.
(66) Neugebauer; Scheffler. *Phys. Rev. B* **1992**, *46*, 16067.
(67) Henkelman, G.; Uberuaga, B.; Jonsson, H. *J. Chem. Phys.* **2000**, *113*, 9901−9904.
(68) Carrasco, J.; Illas, F.; Lopez, N. *Phys. Rev. Lett.* **2008**, *100*, 016101.
(69) Grönbeck, H.; Pana, I. *Phys. Rev. B* **2008**, *77*, 245419.
(70) Guhl, H.; Miller, W.; Reuter, K. *Phys. Rev. B* **2010**, *81*, 155455.
(71) Chakarova-Käck, S. D.; Schröder, E.; Lundqvist, B. I.; Langreth, D. C. *Phys. Rev. Lett.* **2006**, *96*, 146107.
(72) Puzder, A.; Dion, M.; Langreth, D. C. *J. Chem. Phys.* **2006**, *124*, 164105.
(73) Ziambaras, E.; Kleis, J.; Schröder, E.; Hyldgaard, P. *Phys. Rev. B* **2007**, *76*, 155425.
(74) Hamada, I. *J. Chem. Phys.* **2010**, *133*, 214503.
(75) Lee, K.; A. K. Kelkkanen, K. B.; Andersson, S.; D. C. Langreth, E. S.; Lundqvist, B. I.; Hyldgaard, P. *Phys. Rev. B* **2011**, *84*, 193408.
(76) Marrocchelli, D.; Yildiz, B. *J. Phys. Chem. C* **2012**, *116*, 2411−2424.

(77) Fuente, S.; Branda, M. M.; Illas, F. *Theor. Chem. Acc.* **2012**, *131*, 1190.
(78) Molinari, M.; Parker, S. C.; Sayle, D. C.; Islam, M. S. *J. Phys. Chem. C* **2012**, *116*, 7073.

NOTE ADDED IN PROOF

We have become aware of two very recent references (refs 77 and 78) that also deal with the problem of water adsorption and dissociation on ceria surfaces.